

# Characteristics and filtering of low-frequency artificial short deletion variations based on nanopore sequencing

Fuqiang Ye<sup>1,\*,†</sup>, Juanjuan Zhu<sup>2,\*,†</sup>, Xiaomin Zhang<sup>3,\*,†</sup>, Jiarong Zhang<sup>3,4</sup>, Zihan Xie<sup>3,5</sup>, Tingting Yang<sup>3,4</sup>, Yifang Han<sup>1</sup>, Xiaohong Yang<sup>1</sup>, Zilin Ren<sup>6,7,\*</sup>, and Ming Ni<sup>6,3,\*</sup>

<sup>1</sup>Huadong Research Institute for Medicine and Biotechniques, Nanjing 210002, People's Republic of China

<sup>2</sup>School of Life Science and Technology, China Pharmaceutical University, Nanjing 211198, People's Republic of China

<sup>3</sup>Department of Advanced & Interdisciplinary Biotechnology, Academy of Military Medical Sciences, Beijing 100850, People's Republic of China

<sup>4</sup>School of Forensic Medicine, Shanxi Medical University, Jinzhong 030600, People's Republic of China

<sup>5</sup>College of Life Science and Technology, Beijing University of Chemical Technology, Beijing 100029, People's Republic of China

<sup>6</sup>Changchun Veterinary Research Institute, Chinese Academy of Agricultural Sciences, State Key Laboratory of Pathogen and Biosecurity, Key Laboratory of Jilin Province for Zoonosis Prevention and Control, Changchun 130122, People's Republic of China

<sup>7</sup>School of Information Science and Technology, Northeast Normal University, Changchun 130117, People's Republic of China

\*Correspondence address. Zi-lin Ren, E-mail: [zilin.ren@outlook.com](mailto:zilin.ren@outlook.com); Ming Ni, E-mail: [niming@bmi.ac.cn](mailto:niming@bmi.ac.cn)

†Co-first authors.

†Contributed equally to this work.

## Abstract

**Background:** Nanopore sequencing is characterized by high portability and long reads, albeit accompanied by systematic errors causing short deletions. Few tools can filter low-frequency artificial deletions, especially in single samples.

**Results:** To solve this problem, we first synthesized or purchased 17 DNA/RNA standards for nanopore sequencing with R9 and R10 flowcells to obtain benchmarking datasets. False-positive (FP) deletions were prevalent (75.86%–96.26%), while the majority (62.07%–79.68%) were located in homopolymeric regions. The 10-mer base-quality scores (Q scores) and sequencing speeds flanking the FP homopolymeric deletions marginally differed from the true-positive (TP) deletions. We thus investigated the raw current signals after normalizing them by length. We found more significant differences in current signals between the reads with and without FP deletions. Indexes including the MRPP A (Multiple Response Permutation Procedure, statistic A), the accumulative difference of normalized current signals, and the Q score were tested for the power of distinguishing between FP and TP deletions. MRPP A outperformed the other indexes in homopolymeric regions and achieved the highest accuracy of 76.73% for challenging 1-base homopolymeric deletions. When sequencing depth was low, the Q score performed better than MRPP A. We developed Delter (Deletion filter) to filter low-frequency FP deletions of nanopore sequencing in single samples, which removed 60.98% to 100% of artificial homopolymeric deletions in real samples.

**Conclusions:** Low-frequency artificial short deletion variations, especially the most challenging homopolymeric deletions, could be effectively filtered by Delter using normalized current signals or Q scores according to the employed sequencing strategies.

**Keywords:** nanopore sequencing, low-frequency deletions, filtering

## Introduction

Nanopore sequencing is distinguished by its high portability, compared to other commercially available sequencing technologies such as the single-molecule real-time (SMRT) sequencing by PacBio and massive parallel sequencing (MPS) by Illumina and MGI Tech. The smallest sequencer now is the MinION Mk1B (Oxford Nanopore Technologies), which weighs only 87 grams. It can yield Gb-level sequencing data in a single run and has low requirements for environmental conditions. These features make MinION Mk1B well suited for in-field sequencing applications such as viral genomic surveillance during epidemics and biodiversity surveillance [1–3]. On the other hand, the lengths of nanopore sequencing reads are primarily determined by the DNA or RNA molecules passing through nanopores. Nanopore sequencing is widely used for genome and transcriptome assembling [4–11] and long haplotype phasing [12, 13].

Despite the benefits in portability and sequencing length, nanopore sequencing still exhibits relatively higher noise than

MPS and SMRT sequencing [14, 15]. Compared to the initial version of nanopore sequencing devices, the accuracy of current sequencers has been notably improved by engineered pore proteins [14, 16] and deep learning-based basecalling tools [14, 17]. Multiple studies have demonstrated that using nanopore sequencing enables the acquisition of reliable consensus genomes and variations for viruses, bacteria, and human [8, 15, 18–21]. However, when heterogeneity of genetic materials exists, such as in viral quasi-species, heterogeneous bacterial colonies, and tumors with heterogeneity, nanopore sequencing still needs improvement in identifying the low-frequency variations [14, 19, 22].

Moreover, nanopore sequencing is more prone to errors in short insertions and deletions (indels), especially in low-complexity regions like homopolymers, compared to single nucleotide variations (SNVs) [23–28]. Cretu Stancu et al. [25] reported a 2.6-fold increase in deletion errors for sequences overlapping with homopolymers. Delahaye et al. [27] found that nearly 50% of nanopore sequencing errors were attributed to homopolymers.

Received: July 29, 2024. Revised: December 20, 2024. Accepted: February 9, 2025

© The Author(s) 2025. Published by Oxford University Press GigaScience. This is an Open Access article distributed under the terms of the Creative Commons Attribution License (<https://creativecommons.org/licenses/by/4.0/>), which permits unrestricted reuse, distribution, and reproduction in any medium, provided the original work is properly cited.

A recent study benchmarked 7 nanopore sequencing basecaller models and observed median homopolymer error rates of 14.9% to 44.5% [28]. The high error rates in homopolymeric regions can impose limitations on the application of nanopore sequencing. For instance, artificial deletion variations with low frequencies ( $<0.5$ ) in cancer-related genomic tests are more prone to be misclassified as pathogenic or likely pathogenic than artificial SNVs. Accurately detecting low-frequency variations is also pivotal in identifying intrahost heterogeneity of pathogens, which is crucial for studying the microevolution, adaption, and recombination of viruses or bacteria [29–31]. Nonetheless, several studies have suggested that nanopore sequencing is unsuitable for detecting intrahost indels and SNVs due to the high levels of low-frequency errors [18, 19].

To date, there is a lack of methods to filter artificial low-frequency variations for nanopore sequencing. Recently, Liu et al. [26] reported a tool named Variabel that employs longitudinal or cross-sectional samples to recover low-frequency intrahost variations. Variabel can identify low-frequency variations with a  $<0.5$  allele frequency, but its performance in differentiating genuine and artificial indels in homopolymeric regions was not assessed. To our knowledge, no method or tool has been proposed for filtering artificial low-frequency indels applicable to single-sample nanopore sequencing. The errors in nanopore sequencing, particularly those in homopolymeric regions, are primarily ascribed to the basecalling process, in which raw electric current singles are converted into nucleotide sequences [28]. It has been reported that a fine-tuned or specially trained model for a selected set of nucleotide sequences could potentially reduce the false-positive rates of basecaller [32]. However, there has been no comprehensive investigation of low-frequency errors in nanopore sequencing.

In this study, we employed the R9 and R10 flow cells and chemistries of nanopore sequencing to sequence synthetic nucleotides. Our results show that  $>96.00\%$  of the artificial variations had a frequency  $<0.3$ , and most (73.00%) were short deletions in homopolymeric regions. We compared the raw current signals, base-quality scores (Q scores), and passing-pore sequencing speeds of the reads with and without deletions and characterized their differences. We developed a tool named Delter (Deletion filter) to distinguish between false and true low-frequency short deletions identified using nanopore sequencing (Fig. 1).

## Materials and Methods

### Synthetic DNA and RNA sequences

Nine SARS-CoV-2 synthetic RNA genome controls (Twist Bioscience), including the wild-type Wuhan-Hu-1 strain (GenBank accession MN908947.3) and variants from Alpha, Beta, Delta, Epsilon, Iota, Kappa, Omicron BA.1, and Omicron BA.2 lineages were purchased (Supplementary Table S1). With the genome of the Wuhan-Hu-1 strain as a reference, other SARS-CoV-2 variants contain 306 deletion variations with lengths ranging from 3 to 9 nucleotides (nts, Supplementary Table S2).

In addition, wild-type and mutated nucleotide sequences of the S gene of SARS-CoV-2 (GenBank accession MN908947.3), Penton gene of human adenovirus subtype 55 (HAdV55, GenBank accession MK886831.1), 16S ribosomal DNA gene of *Escherichia coli* (strain: Castellani and Chalmers 1919,01485 cm, NRRL accession B-1109), and an assembly contig of *Saccharomyces cerevisiae* (strain: *Saccharomyces cerevisiae* Meyen ex E. C. Hansen (1883) ATCC 9763, NRRL accession Y-567) were synthe-

sized in plasmids by Sangon Biotech Co., Ltd. (Supplementary Table S3). The mutated sequences were designed to contain 242 deletions of 1 to 3 nts, which were evenly distributed in homopolymeric and non-homopolymeric regions (Supplementary Table S4).

### Nanopore sequencing and basecalling

SARS-CoV-2 synthetic RNA controls were reversely transcribed with the Whole Transcriptome Amplification Kit (cat. 207043; Qiagen) following the manufacturer's instruction. The cDNA products and synthetic DNA plasmids were employed as inputs to prepare libraries with the Rapid Barcoding Kit (SQK-RBK004; Oxford Nanopore Technologies) and sequenced by using a MinION Mk1B sequencer with the R9.4.1 (FLO-MIN106; Oxford Nanopore Technologies) and R10.4.1 flow cells (FLO-MIN114; Oxford Nanopore Technologies) according to the manufacturer's protocols.

The MinKNOW software (v22.03.5, v22.08.9, or v22.10.10; Oxford Nanopore Technologies) was employed to the sequencing run, and Guppy (v6.0.6, v6.2.11, or v6.3.9; Oxford Nanopore Technologies), an integrated component of MinKNOW, was used for basecalling throughout sequencing runs. For sequencing with R9.4.1 flow cells, re-basecalling was conducted using Guppy (v6.2.1; [RRID:SCR\\_023196](#)) with the super accuracy (SUP) model. For the R10 sequencing run, the fast, high-accuracy (HAC), and SUP basecalling models were utilized.

### Quality control and alignment of basecalled reads

The sequencing adapters were trimmed by using Porechop (v0.2.4; [RRID:SCR\\_016967](#)). NanoFilt (v2.8.0; [RRID:SCR\\_016966](#)) [33] was then used to filter reads with undesirable lengths and low-quality scores ( $-q\ 8$  --length 100) and to trim 10 bases from 5'/3' ends of the reads. Minimap2 (v2.24, [RRID:SCR\\_018550](#)) [34] was used for alignment of clean reads to reference sequences, with the pre-set parameters for nanopore sequencing data (-ax map-ont). Samtools (v1.13; [RRID:SCR\\_005227](#)) [35] was employed for downstream analyses of the alignments. The unmatched fragments marked as soft-clipped in the BAM file of aligned reads were trimmed using in-house scripts.

### Variation calling and filtering

Nanopore sequencing variations were identified using LoFreq2 (v2.1.5, [RRID:SCR\\_013054](#)), which is applicable for analyzing nanopore sequencing data to detect low-frequency variations [36]. First, with the "lofreq indelqual" parameter, indel quality scores were added to the BAM files. Then, the "lofreq call-parallel" command was used to call variations with the following parameters: "--no-default-filter --call-indels." The candidate variations were filtered using the "lofreq filter" command with parameters of "lofreq filter --cov-min 100 --af-min 0.05 --sb-alpha 0.01 --sb-incl-indels." For sequencing data of synthetic SARS-CoV-2 controls that underwent whole transcriptome amplification, variations were also identified using VarScan2 (v2.4.4; [RRID:SCR\\_006849](#)) [37] and Medaka (v1.7.3) [38] with default parameters. Clair3 (v1.0.10; [RRID:SCR\\_026063](#)) [39] and NanoCaller (v3.6.0) [40] were employed for comparison of different variant callers.

### Aligning electric current signals to ground-truth nucleotide sequences

The raw R9 sequencing data containing the electric current signal-level data (current signals or squiggles) and the asso-

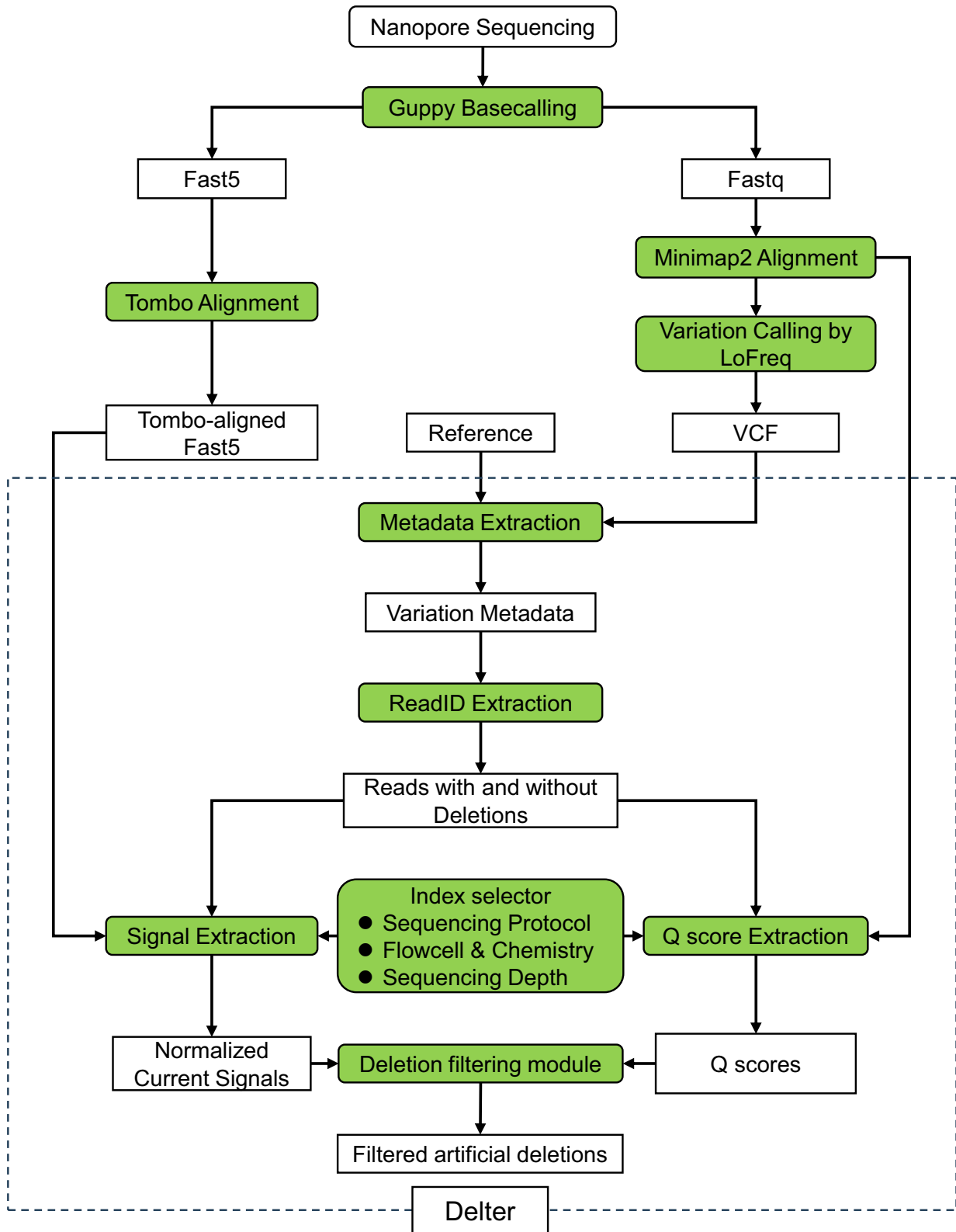


**Figure 1:** Workflow of Delter for filtering FP deletions in R9 and R10 nanopore sequencing. Delter is organized as a Snakemake workflow. It is composed of 6 functional modules: (i) metadata extraction module, (ii) ReadID extraction module, (iii) index selector, (iv) signal extraction module, (v) Q score extraction module, and (vi) deletion filtering module. Details are listed in the “Materials and Methods” section.

ciated basecalls were stored in “fast5” formatted files. The “multi\_to\_single\_fast5” command from the ont-fast5-api Python package (v4.1.1) [41] was performed to split multiple-read fast5 files into single-read fast5 files. Then, Tombo (v1.5.1; [RRID:SCR\\_024388](#)) was utilized to load the single-read fast5 file and assign current measurements in the squiggle to each base of the read via alignment to the reference sequence with the “resquiggle” command.

The squiggles of 10 bases or 20 bases flanking each variation were extracted using in-house scripts to compare between reads with and without artificial deletions. As the sampling rate of the MinION sequencer is 4,000 times per second, the time interval between 2 consecutive current measurements in the squiggle is fixed. The real-time sequencing or translocation speed of the DNA molecules passing through the nanopores (number of current measurements per base) was determined by dividing the number of current measurements (signal lengths) of the relevant read fragments by the number of bases.

The passing-pore sequencing speeds of DNA molecules are highly diverse. Namely, the same number of nucleotides can produce different lengths of current signals. Therefore, before further analysis, these current signals were normalized by length using a binning approach. The mean values of the current measurements assigned to the same bin were utilized. The sums of difference values (accumulative differences) between the normalized signals of reads with and without deletions were also calculated.

### Subsampling approach to determine thresholds

Our method was evaluated under different sequencing depths using a subsampling approach. For each variation, we randomly chose *N* (range: 20 to 2,000) forward- and reverse-aligned reads supporting the reference and nonreference alleles, respectively—namely, *N* forward-aligned reads supporting the reference allele, *N* reverse-aligned reads supporting the reference allele, *N* forward-aligned reads supporting the nonreference allele, and *N* reverse-aligned reads supporting the nonreference allele (strand-specific sequencing depth). Thus, 80 to 8,000 aligned reads per variation were subsampled when available. The areas under the curve (AUCs), sensitivities, and specificities corresponding to each sequencing depth were calculated. The threshold with the highest sum of sensitivity and specificity was used as the default threshold for filtering.

### Statistical analyses and visualization

The R project (v4.2.2) [42] was employed for the statistical analyses and visualization. To compare the normalized signals with equal lengths from reads with and without variations, we used 3 intergroup difference analysis methods, including analysis of similarities (ANOSIM), multiresponse permutation procedure (MRPP), and permutational multivariate analysis of variance (ADONIS2). The R package Vegan (v2.6–4; [RRID:SCR\\_011950](#)) was utilized for the ANOSIM, MRPP, and ADONIS2 calculation. The Kruskal–Wallis rank-sum test was used for intergroup comparison. *P* values were adjusted with the Benjamini and Hochberg method when necessary. The receiver operating characteristic (ROC) curve analysis was conducted to assess the performance of filtering artificial variations using the R package pROC (v1.18.2; [RRID:SCR\\_024286](#)). The R packages ggplot2 (v3.4.1; [RRID:SCR\\_014601](#)), ggpubr (v0.6.0; [RRID:SCR\\_021139](#)), ggsci (v2.9) [43], and ComplexHeatmap (v2.14.0; [RRID:SCR\\_017270](#)) were implemented for visualization.

### Implementation of the filter for removing artificial deletions

Delter is organized as a Snakemake workflow. It is composed of 6 functional modules: (i) metadata extraction module. This module uses a variant call format (VCF) file output by LoFreq and reference sequence as inputs to generate the variation metadata, including deletion type (homo-dels or other-dels), deletion length, and the starting and ending positions. (ii) ReadID extraction module. Its main function is to get read lists containing deletions and no deletions. (iii) Index selector. This core module automatically selects appropriate index(es) depending on the sequencing protocol, flowcell/chemistry, and sequencing depth. (iv) Signal extraction module. If MRPP A is chosen for downstream analyses, this module will extract the raw current signals of *N* bases flanking each deletion variation, which are preprocessed to normalized current signals using a binning approach. (v) Q score extraction module. If Q score is selected, it will output base qualities of the 10-mer read region of deletion variations. (vi) Deletion filtering module. This module bundles several functions to calculate MRPP A and average 10-mer Q scores. It also filters and marks artificial deletions in the final output.

The filter takes several files as inputs: (i) the VCF file output by LoFreq, (ii) the sorted BAM files storing alignment of nanopore reads to the reference sequence, (iii) the reference sequence, and (iv) the directory storing Tombo-resquiggled single-read fast5 files when R9 flow cell and chemistry are employed. Users should also provide the sequencing protocol (amplicon or direct), flowcell/chemistry (R9 or R10), strand-specific sequencing depth for subsampling, the directory storing the final results, and the base number flanking each variation to extract Q scores and current signals.

### External validation using real samples

Our method was validated in sequencing data of human adenovirus (HAdV) and microbial standard samples. We first synthesized plasmids containing full-length Fiber, Penton, and Hexon genes from different HAdV subtypes, including HAdV11, 14, and 55 (*n* = 7; [Supplementary Table S5](#)). These genes natively contain 5 real deletions when compared to references. Partial gene fragments (amplicons) covering true deletions were also amplified using PCR primers (*n* = 9). The samples were mixed and sequenced using R9.4.1 flow cell (*n* = 9). ZymoBIOMICS Gut Microbiome Standard (cat. D6331; Zymo Research) containing varying bacterial cell contents was further sequenced with R9.4.1 flow cell and processed. As these bacteria should not have any true variations, all of the variations output by LoFreq are identified as negative. In order to assess the applicability of the tool for metagenomic scenarios, we also evaluated the pipeline in case of the coexistence of closely related bacterial strains. The microbial standard D6331 contains 5 strains of *Escherichia coli*: namely, B-1109, B-766, B-2207, B-3008, and JM109. We randomly selected the strain B-1109 as the reference genome and then evaluated the similarities between the other 4 strains and the reference using fastANI (v1.33; [RRID:SCR\\_021091](#)). The average nucleotide identities range from 98.46% to 99.52%. DNAdiff (v1.3) and GSAAlign (v1.0.22) [44] were employed to call variations of each strain relative to the reference B-1109 separately. The shared deletion variations reported by both tools were merged to constitute a list of true deletions (*n* = 236). The D6331 nanopore sequencing data were then aligned to the B-1109 reference genome. The VCF was called with LoFreq and used as input for the Delter workflow.



Moreover, 3 public datasets available on the NCBI SRA database were included for further assessment. The African swine fever virus (ASFV) dataset has 1 Nanopore R10 run and 4 paired Illumina MiSeq runs (NCBI accession number: PRJNA1096272). The *Pseudomonas aeruginosa* PAO1 dataset contains R10 SUP data generated by GridION (SRA accession number: ERR958864) and paired MiSeq data (ERR9285397). As the GridION dataset has a large number of reads ( $n > 630,000$ ), only the first 120,000 reads were selected for downstream analyses. The *Brucella suis* dataset has paired Nanopore R9 (ERR10828735) and Illumina MiSeq (ERR10820713) sequencing data. After quality control with NanoFilt (nanopore data) or fastp (MiSeq data, v0.22.0; [RRID:SCR\\_016962](#)), all the sequencing data were aligned to the reference genome of ASFV (NC\_044945.1), *P. aeruginosa* PAO1 (NC\_002516.2), or *B. suis* (NC\_004310.3) with Minimap2 or bwa (v0.7.17; [RRID:SCR\\_010910](#)). For Illumina datasets, variations were called using LoFreq with a minimum depth of 20 and a minimum allele frequency of 0.05. Variation calls on Illumina sequencing runs were used as real variations. For nanopore datasets, variations were called using the same parameters as mentioned above.

## Results

### Nanopore sequencing of synthetic samples

We obtained a total of 17 chemically synthesized RNA and DNA samples for nanopore sequencing, covering both wild types and the corresponding mutants ([Supplementary Tables S1–S4](#)). Nine synthetic RNA samples (~30 kb) were SARS-CoV-2 standards, among which 8 are variants of interest or concern. Due to their low copy numbers (5,000 copies per standard), they underwent whole transcriptome amplification (WTA) before nanopore sequencing (referred to as WTA sequencing). Eight synthetic DNA samples contained the sequences from SARS-CoV-2, human adenovirus subtype 55 (HAdV55), *E. coli*, and *S. cerevisiae* (length ranged from 1,468 to 1,674), and the mutants carried designed deletion variations. The mutants and their corresponding wild types were respectively mixed with ratios of 1:9, 1:4, and 1:1 to mimic low-frequency variations ([Supplementary Fig. S1](#)). The synthetic DNA samples from plasmids were directly sequenced without amplification (referred to as direct sequencing). Three independent sequencing runs containing 33 synthetic samples were conducted using the MinION sequencer Mk1B with R9 and R10 flow cells, and a total of 9.3 Gb clean sequencing data were yielded after quality control ([Supplementary Table S6](#)). WTA sequencing samples generated shorter reads (N50: 1,137–1,656 bases) than direct sequencing ones (N50: 4,131–4,349 bases).

### The majority of artificial variations were deletions

Small variations with a  $\geq 0.05$  mutated allele frequency (MuAF) were identified for data generated by WTA sequencing and direct sequencing with R9 and R10 flow cells. The recall rates of true-positive (TP) variations were high, which were 99.67% (305 of 306) for the WTA sequencing and 97.80% (R9, 710 of 726) to 98.07% (R10, 712 of 726) for the direct sequencing. Most false negatives were attributed to low sequencing depth or marginal MuAFs near the 0.05 threshold.

Abundant artificial (false positive, FP) low-frequency variations were identified (Fig. 2A–C). Among all the FP types, the small deletions located in  $\geq 3$ -base homopolymeric regions (denoted as homo-dels) were remarkably dominating (62.07%–79.68%), followed by the deletions in the non-homopolymeric regions (other-

dels, 10.40%–16.58%). FP insertions and SNVs took a relatively small proportion of all the FPs. Most FP SNVs of WTA sequencing could be filtered by trimming of read ends [18, 19]. We trimmed 10 bases from both ends of the aligned fragment of reads and reduced 77.11% FP SNVs of WTA sequencing (Fig. 2A). Other-dels and insertions were also reduced (22.93% and 14.89%, respectively), whereas only 0.59% FP homo-dels were excluded by the trimming (Fig. 2A). In contrast, the trimming led to higher FP ratios in direct sequencing samples (Fig. 2B, C), which might be due to the increase of marginal MuAFs to  $> 0.05$ . This result was consistent using different variant callers ([Supplementary Fig. S2](#)). Different basecalling models (fast, HAC and SUP) led to diverse FP ratios in R10 direct sequencing samples (Fig. 2C; [Supplementary Fig. S3](#)). The samples sequenced with R10 flow cell generated fewer FP variations than those with R9 flow cell (SUP: 24/172 = 13.95%; HAC: 85/172 = 49.42%).

We also investigated how the FP ratios varied as the MuAF thresholds grew. As shown in Fig. 2D, different sequencing strategies had similar trends. The majority ( $> 96.00\%$ ) of FP variations had a low MuAF  $< 0.3$ . FP variations were usually shared in the datasets of highly homologous samples with identical sequencing strategies. In the WTA sequencing dataset of the SARS-CoV-2 standards, a total of 233 genomic loci were found to have FP variations, of which 25.32% and 47.21% were identified in all or at least 50% of samples (Fig. 2E). For the direct sequencing samples, the same FP variations were also identified in mixtures derived from different mutant/wild-type ratios (Fig. 2F, G). There were 14 homo-dels shared by both R9 and R10 direct sequencing samples, while none of other-dels or insertions were shared, indicating the inherent systematic errors in nanopore sequencing despite the flow cell and chemistry.

### A biased Q score and sequencing speed distribution of FP deletions compared to TP deletions

Deletion variations comprised the highest proportion, while SNVs and insertions were relatively low, so we focused mainly on homo-dels and other-dels. The 10-mer average Q scores (upstream and downstream of 5 bases) flanking each variation were calculated to compare between reads with and without deletions. Reads containing FP homo-dels and other-dels had lower Q scores than reads with no deletions (Fig. 3A–C, [Supplementary Fig. S4A](#)). In contrast, reads containing TP deletion variations had a nearly identical distribution of Q scores relative to reads without deletions. FP homo-dels from different sequencing strategies had diverse Q score distribution compared to other-dels. Moreover, the differences between reads with and without deletions were negligible in the FP homo-dels derived from R10 direct sequencing samples basecalled with the fast basecalling model ([Supplementary Fig. S4B](#)). Notably, the differences between reads with and without homo-dels were minor relative to those in other-dels, which indicated the difficulty in distinguishing between FP homo-dels and TP deletions.

High room temperature could lead to abnormal translocation speeds of templates going through nanopore proteins and further generate poorer base qualities. We thus analyzed the sequencing speeds of FP and TP deletions. The electric current signal-level data (current signals or squiggles) of 10 or 20 bases (10-mer or 20-mer current signals) flanking each deletion variation were extracted. FP deletion variations were observed to have fewer numbers of current measurements (sampling points) per base, namely, higher sequencing speeds, than reads without deletions (Fig. 3D,

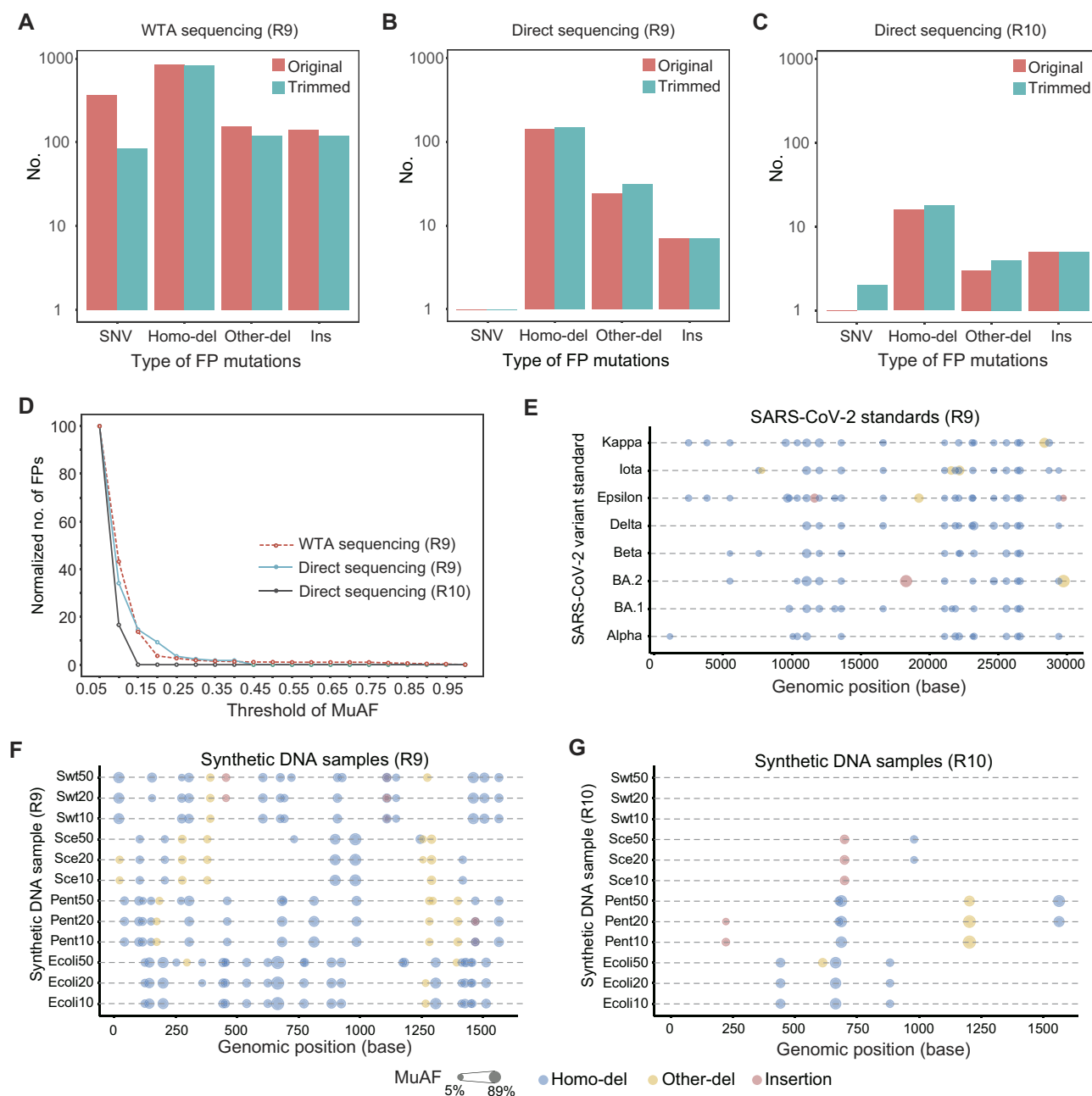


**Figure 2:** False-positive variations in different sequencing strategies with ONT R9 and R10 flow cells and chemistries. (A–C) The bar plots of 4 types of artificial variations before (red) and after (blue) trimming bases in ONT R9 WTA sequencing data (A), R9 direct sequencing data (B), and R10 direct sequencing data basecalled with the SUP model (C). The y-axis was  $\log_{10}$  transformed. (D) The normalized FP counts at each MuAF threshold relative to those at MuAF = 0.05. (E–G) The genomic distributions of FP variations in R9 WTA sequencing data (E), R9 direct sequencing data (F), and R10 direct sequencing data basecalled with the SUP model (G); only deletions and insertions were plotted. FP variations with MuAF  $\geq 0.15$  in SARS-CoV-2 variants were selected to display for better visualization. Swt: wild-type SARS-CoV-2; Ecoli: *Escherichia coli*; Pent: human adenovirus subtype 55; Sce: *Saccharomyces cerevisiae*.

E). In contrast, TP deletion variations differed slightly from reads without deletions. At the scale of whole read, FP and TP deletion variations had no significant differences in sequencing speeds (Supplementary Fig. S5).

### Remarkable differences between current signals of R9 FP and TP deletions

Although FP deletions had more significant differences in Q score than sequencing speed, the Q score alone might be insufficient to separate FP homo-dels from true deletions in R9 sequencing

data. As Q scores were directly correlated with the basecalling of current signals, we further characterized the raw signals of FP and TP deletions.

The 10-mer current signals flanking FP deletion variations were further processed to inspect whether remarkable differences exist when compared to reads without deletions. As the counts of current measurements (signal lengths) of each variation were not equal and sequencing speeds had no close relationship with FP or TP deletions, the current signals first underwent binning-based normalization preprocesses to even lengths. The current mea-

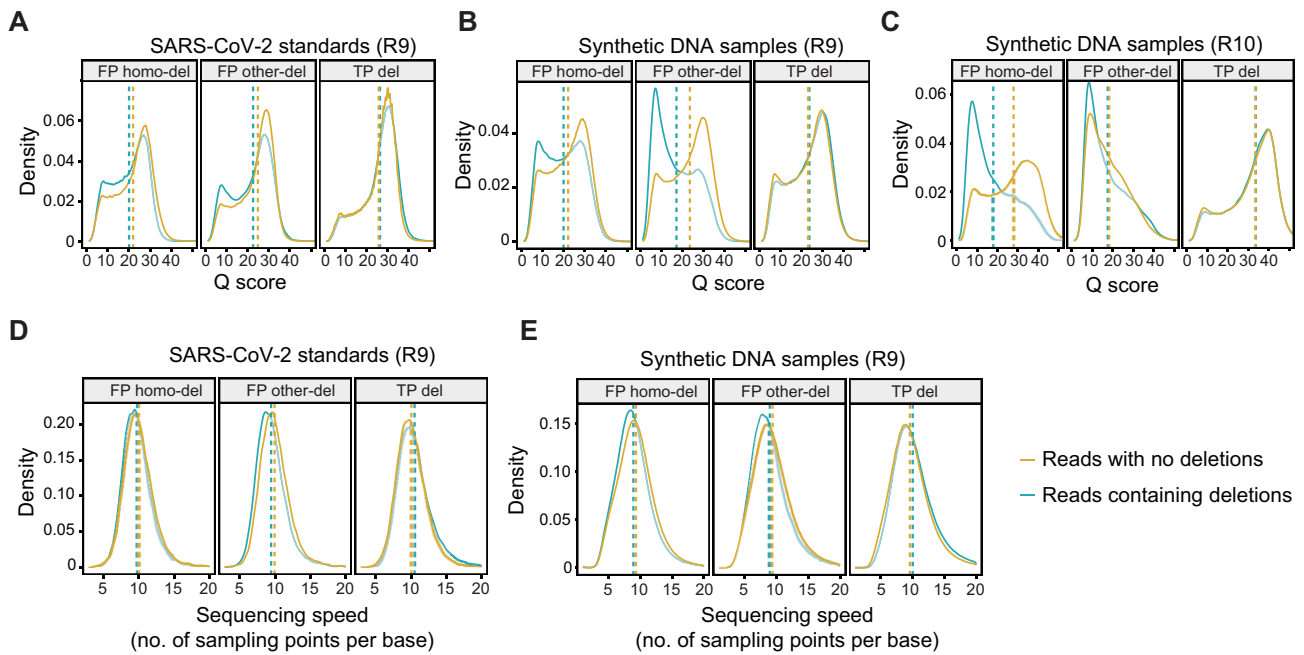


**Figure 3:** The characteristics of Q score and sequencing speed of FP variations. (A–C) The comparisons of Q scores between reads containing deletion variations and reads with no deletions in R9 WTA sequencing data (A), R9 direct sequencing data (B), and R10 direct sequencing data basecalled with the SUP model (C). The dashed lines represent the mean values of Q scores. (D, E) The comparisons of sequencing speeds between reads containing deletion variations and reads with no deletions in R9 WTA sequencing data (D) and R9 direct sequencing data (E). The dashed lines represent the mean values of speeds. Sequencing speed equals the division of the number of current measurements by the base number.

measurements in each bin were then averaged. The current signals of reads supporting FP deletion variations had slight differences relative to reads without deletions, regardless of homo-dels or other-dels (Fig. 4A and [Supplementary Fig. S6A](#)). However, TP deletions had remarkable discrepancies between reads with and without deletions (Fig. 4B and [Supplementary Fig. S6B](#)). Notably, the differences enlarged as the deletion types varied from homo-dels to other-dels. Moreover, the differences grew bigger when more bases were deleted. The sums of difference values (accumulative differences) between the normalized signals of reads with and without deletions were then calculated. FP deletions were observed to have lower sums than TP deletions (Fig. 4C–F), and homo-dels had lower sums than other-dels ([Supplementary Fig. S7](#)). The differences between TP and FP deletions in current signals were more significant than those observed in Q score and sequencing speed.

The normalized equal signal lengths were also suitable for downstream intergroup difference detection methods. ANOSIM, MRPP, and ADONIS2, which are widely used in ecological and metagenomic analyses, were employed to compare the signal distribution pattern. The ANOSIM statistic R, MRPP statistic A, and ADONIS2 statistic F were also calculated. Compared with ANOSIM R, ADONIS2 F, and accumulative signal difference, MRPP A had the largest fold changes between TP and FP deletion variations (Fig. 4G, H). It is also observed that FP deletion variations had lower MRPP A values than TP deletions (Fig. 4I–L). Thus, MRPP could be used in downstream analysis to filter artificial deletion variations.

### Performance assessment of MRPP A, Q score, and accumulative difference in identifying artificial deletions

The ROC curves were employed to assess the effects of 3 indexes, MRPP A, Q score, and accumulative difference, on distinguishing between FP and TP deletions. In WTA sequencing data, the MRPP

A obtained the highest AUC of 0.98 (accuracy: 91.60%) in distinguishing between artificial and true variations ([Supplementary Fig. S8A](#)). In R9 direct sequencing samples, the MRPP A outperformed the Q score and the accumulative difference in homopolymeric regions, whose AUCs were 0.85, 0.76, and 0.80, respectively (Fig. 5A and [Supplementary Fig. S8B](#)). For the most challenging artificial 1-base homopolymeric deletions (Fig. 5B), MRPP A achieved the highest accuracy of 76.73% compared with the Q score (69.90%) and the sum of difference (71.39%). For other artificial deletions, MRPP A achieved an AUC of 0.92 and an accuracy of 83.41% (Fig. 5C). Moreover, MRPP A also had higher AUCs than ANOSIM R and ADONIS2 F ([Supplementary Fig. S9](#)).

For R10 direct sequencing samples, the Q score was utilized to separate FP from TP deletions under different basecalling models. In the fast basecalling model, Q scores had the weakest performance in distinguishing between FP and TP deletion variations ([Supplementary Fig. S10](#)), indicating its inapplicability in filtering FP deletion variations. The SUP and HAC models generated fewer FP deletions with higher AUCs (SUP: 0.99–1; HAC: 0.89–0.98) (Fig. 6, [Supplementary Fig. S11](#)). For other-dels, the Q score had a higher AUC than homo-dels. Using the Q score alone has achieved a better performance than MRPP A, which is used in R9 data (AUC: 0.81–0.92), as revealed by the ROC analyses. Thus, it is sufficient to employ the Q score to filter FP deletion variations for R10. We found average Q scores below 22 could discriminate between FP and TP deletions, which enabled the identification of 90.63% artificial homo-dels (accuracy: 96.88%) and 100% other-dels (accuracy: 100.00%).

### Implementation of the filtering tool for FP deletions from R9 and R10 nanopore sequencing

The performance of our method was checked under different sequencing depths. MRPP A achieved stable AUCs with strand-

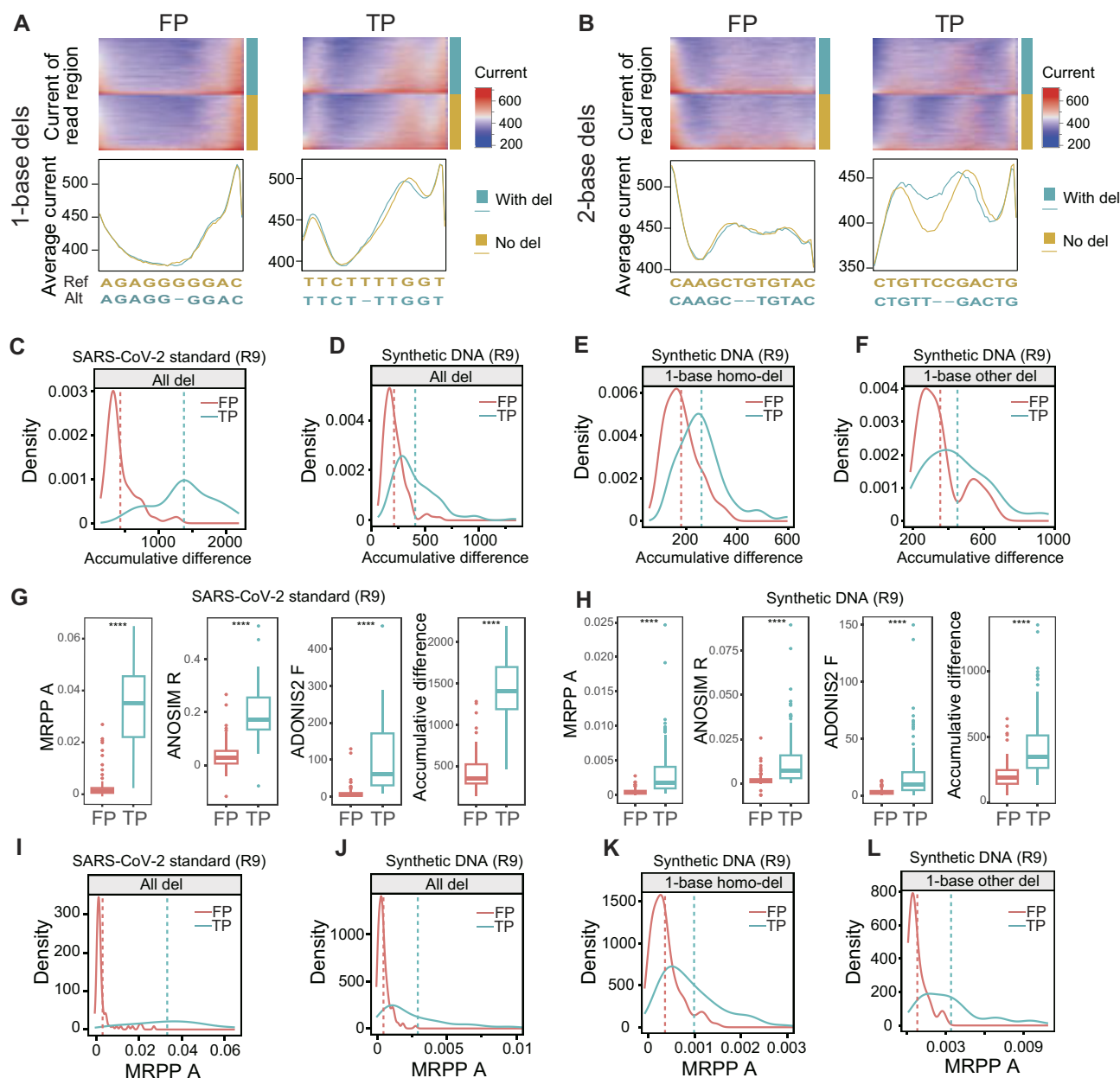


**Figure 4:** The features of normalized current signals in R9 sequencing data. (A) Heatmaps of normalized current signals from reads with and without 1-base FP and TP homo-del variations. The line plots represent each column's average normalized current measurements in the heatmap. The alternate alleles corresponding to deletions are displayed. (B) Heatmaps of normalized current signals from reads with and without 2-base FP and TP other-del variations. (C) The accumulative difference of average normalized current measurements from FP and TP deletions in R9 WTA sequencing data. For each deletion variation, the accumulative difference equals the sum of the difference current values of normalized current measurements between reads with and without deletions. (D–F) The accumulative difference of average normalized current signals corresponding to all deletions (D), 1-base homo-dels (E), and 1-base other-dels (F) in R9 direct sequencing data. The dashed lines represent the mean values. (G, H) The boxplots of MRPP A, ANOSIM R, ADONIS2 F, and accumulative signal difference in FP and TP deletions in R9 WTA sequencing data (G) and R9 direct sequencing data (H). Boxes represent the interquartile range (IQR) between the first and third quartiles (25th and 75th percentiles, respectively). Lines inside denote the median, and whiskers denote the most extreme values within 1.5 times the IQR from the first and third quartiles. Outlier values are represented as points. \*\*\*\* $P \leq 0.0001$ . (I) The density plot of MRPP A corresponding to FP and TP deletions in R9 WTA sequencing data. (J–L) The density plot of MRPP A corresponding to all deletions (J), 1-base homo-dels (K), and 1-base other-dels (L) in R9 direct sequencing data. The dashed lines represent the mean values.

specific sequencing depths  $\geq 100\times$  in WTA sequencing data (Supplementary Fig. S12A). For R9 direct sequencing samples, MRPP A began to outperform the Q score at  $400\times$  except in other-del variations (Fig. 7A, B, Supplementary Fig. S12B, C). Thus, MRPP A or Q score would be utilized to filter FP deletions with varied sequencing depths. The Q score could distinguish between FP and TP variations with strand-specific sequencing depths  $\geq 20\times$  in R10

sequencing samples (Supplementary Fig. S12D). The corresponding thresholds of MRPP A or Q score were further determined (Table 1). We then developed a tool named Delter to filter artificial deletion variations from R9 or R10 sequencing data, which could choose an appropriate index depending on sequencing protocol, flow cell, and depth. Variations with indexes lower than the recommended thresholds would be predicted as artificial deletions.



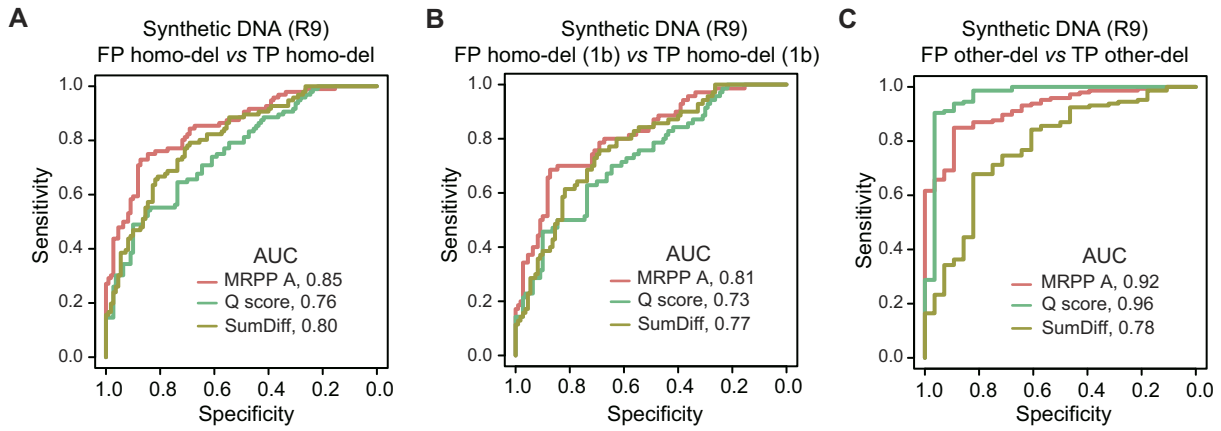


**Figure 5:** Performance assessment of different indexes in distinguishing between FP and TP deletions in R9 direct sequencing samples. (A–C) The ROCs of MRPP A, Q score, and accumulative difference in distinguishing between FP and TP homo-dels (A), between FP and TP 1-base homo-dels (B), and between FP and TP other-dels (C). 1b: 1 base; SumDiff: sum of difference.

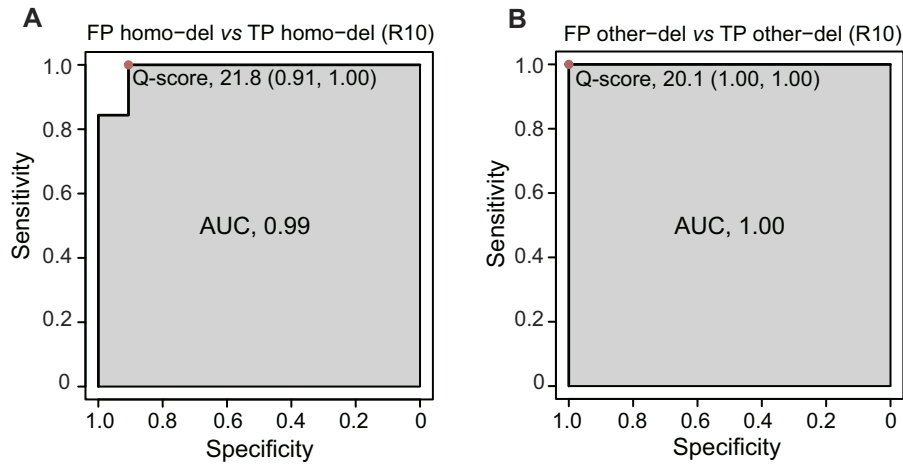


**Figure 6:** Performance assessment of Q score in distinguishing between FP and TP deletions in R10 direct sequencing samples. (A) The ROC of Q score in distinguishing between FP and TP homo-dels. (B) The ROC of Q score in distinguishing between FP and TP other-dels. The best threshold, specificity, sensitivity, and AUC of the SUP model were plotted.

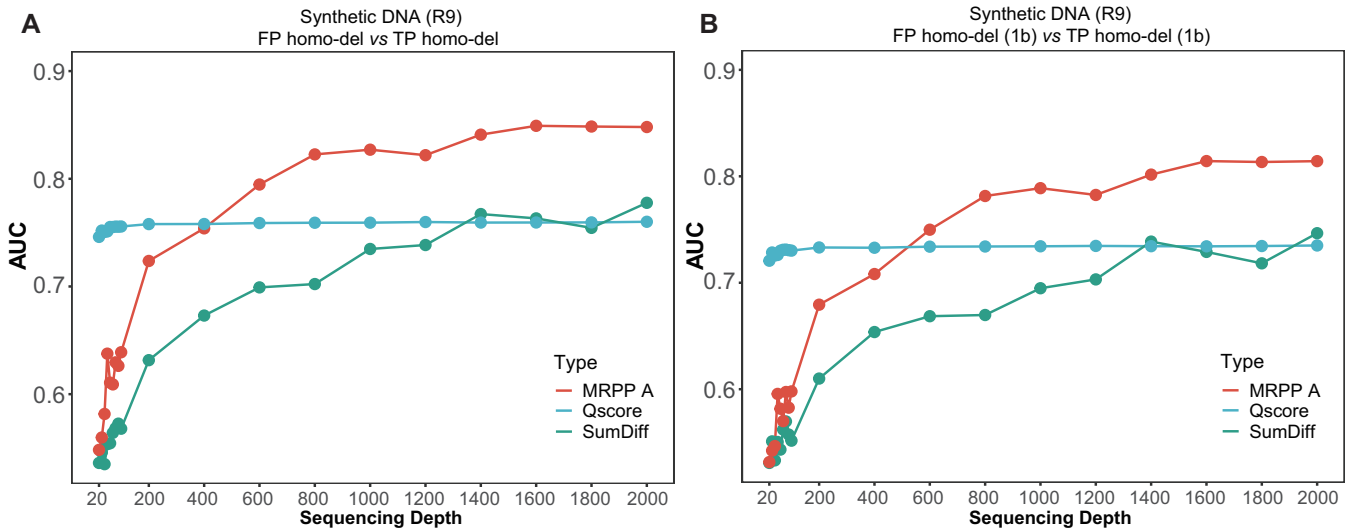


**Figure 7:** The AUCs distinguishing between TP and FP variations across different sequencing depths. (A, B) The MRPP A- and Q score-derived AUCs corresponding to homo-dels (A) and 1-base homo-dels (B) in R9 direct sequencing data. 1b: 1 base; SumDiff: sum of difference.

**Table 1:** The suggested index and threshold across different sequencing protocol, flowcell/chemistry, and depth

Flowcell/chemistry	Sequencing protocol	Sequencing depth*	Index	Threshold
R9	WTA sequencing	≥20×	MRPP A	0.01
	Direct sequencing	≥400×	MRPP A	0.001
	Direct sequencing	[20×,400×)	Q score	23 (homo-del) 20.6 (other-del)
R10	Direct sequencing	≥20×	Q score	21.8 (SUP, homo-del) 20.0 (SUP, other-del)

\*Strand-specific sequencing depth.

**Table 2:** Validation of the filtering method in real samples

Sample	Deletions/homo-deletions before filtering		Deletions/homo-deletions after filtering		Sensitivity	Specificity	Accuracy
	TP	FP	TP	FP			
HAdV full-length gene mixtures (n = 4)	5/0	79/69	5/0	10/6	100.00%/—	87.34%/91.30%	88.10%/91.30%
HAdV amplicon mixtures (n = 5)	5/0	27/23	4/0	0/0	80.00%/—	100.00%/100.00%	96.88%/100.00%
D6331 <i>E. coli</i>	130/27	14,275/12,843	95/12	1,600/829	73.08%/44.44%	88.79%/93.55%	88.65%/93.44%
<i>Veillonella rogosae</i>	0/0	5,930/5,597	0/0	437/382	—/—	92.63%/93.17%	92.63%/93.17%
<i>Bacteroides fragilis</i>	0/0	3,535/3,477	0/0	509/478	—/—	85.60%/86.25%	85.60%/86.25%
<i>Faecalibacterium prausnitzii</i>	0/0	431/429	0/0	46/46	—/—	89.33%/89.28%	89.33%/89.28%
<i>Prevotella corporis</i> genome 1	0/0	684/660	0/0	131/127	—/—	80.85%/80.76%	80.85%/80.76%
<i>Brucella suis</i>	1/0	52/44	1/0	13/6	100.00%/—	75.00%/86.37%	75.47%/86.37%
African swine fever virus	6/1	70/41	6/1	27/16	100.00%/100.00%	61.43%/60.98%	64.47%/61.90%
<i>Pseudomonas aeruginosa</i> PAO1	2/1	1/1	2/1	0/0	100.00%/100.00%	100.00%/100.00%	100.00%/100.00%

We recorded the computational resources for variation calling with LoFreq and deletion filtering with Delter. The runtime and RAM usage required by LoFreq scales with the total bases (Supplementary Fig. S13 and Table S7). The computational costs of Delter depend on the flow cell, sequencing protocol, and sequencing depth. Delter needs much less runtime and RAM usage in R10 data than R9 data. We found the runtime (0.06–3.93 s/read) and RAM usage (0.07–3.46 MB/read) of Delter scales with the mean number of reads aligned to each variation site in each sample (referred as mean read number; Supplementary Fig. S14 and Table S8). Moreover, the computational resources of basecalling the current signals were also listed (Supplementary Table S9).

### Effective removal of artificial deletions in real samples

Our approach was first validated in 9 samples containing HAdV amplicons (amplicon sequencing) and full-length genes (direct sequencing). In HAdV direct sequencing data, 100% of the true variations (MuAF <0.15) were correctly identified, and 63 of 69 artificial homo-dels (MuAF <0.32) were successfully filtered, achieving an overall accuracy of 91.30% (Table 2). In HAdV amplicon sequencing data, 4 of 5 true deletions (MuAF <0.12) were detected, and 100% of the artificial homo-dels (n = 23, MuAF <0.18) were removed. We further tested our method in a microbial standard sample containing *Veillonella rogosae*, *Bacteroides fragilis*, *Faecalibacterium prausnitzii*, *Prevotella corporis*, and 5 strains of *E. coli* (B-1109, B-766, B-2207, B-3008, and JM109). After filtering the results us-

ing the minimum sequencing depth, the removed FP homo-dels in single bacterial strains (*V. rogosae*, *B. fragilis*, *F. prausnitzii*, and *P. corporis*) ranged from 80.76% to 93.17% (MuAF: 0.06–0.70). In addition, the performance of the Delter workflow in the case of coexisting closely related bacterial strains was evaluated in the ZymoBIOMICS Gut Microbiome Standard. When the *E. coli* B-1109 strain was selected as the reference, the shared deletion variations of the other 4 strains (B-766, B-2207, B-3008, and JM109) were merged to constitute a list of true deletions (n = 236). A total of 130 true deletion variations were recalled (MuAF: 0.10–0.85), with 35 (26.92%) misidentified as FP deletions. For the FP deletions (n = 14,275), 12,675 (88.79%, MuAF: 0.08–0.52) were filtered by Delter.

Moreover, 3 public datasets available on the NCBI SRA database were included for further evaluation. In the ASFV dataset (paired Nanopore R10 and Illumina runs), a total of 76 deletions were retained, 6 of which were true deletions (MuAF: 0.69–0.93, accuracy = 100.00%), with 43 FP deletion variations (43/70 = 61.43%, MuAF: 0.05–0.28) being filtered, including 25 FP homo-dels. For the *P. aeruginosa* PAO1 dataset (paired Nanopore R10 and Illumina runs), the genome sequence *P. aeruginosa* PAO1 was selected as the reference. Three deletions were identified, including 2 TP ones (MuAF: 0.21–0.27). The other FP homo-del was successfully filtered by Delter (MuAF = 0.33, accuracy = 100.00%). In the *B. suis* dataset (paired Nanopore R9 and Illumina runs), 53 deletions were retained. Among these deletions, 1 true deletion (MuAF = 0.61, accuracy = 100.00%) was detected. A total of 39 FP deletion variations (39/52 = 75.00%, MuAF: 0.29–0.54) were filtered, among

which 86.37% homo-dels were removed. In summary, these samples proved the efficiency of our filtering method.

## Discussion

Although simplex nanopore sequencing accuracy has increased to Q20+, low-frequency artificial deletion variations still exist in data generated by R9 and R10 flow cells and chemistries, especially in homopolymeric regions. The false-positive variations mainly resulted from systematic sequencing errors and are challenging to eliminate. We aim to remove such artificial deletion variations detected at a MuAF threshold of 0.05. The remarkable differences in sequencing signals and Q scores between artificial and true variations were observed. We then developed the first method to filter artificial deletion variations in single samples via current signals or Q scores according to the sequencing protocols, flowcells, and depth. Our approach focuses on artificial deletions with MuAF as low as 0.05, and it cannot handle false-positive SNVs or insertions of interest at present, which warrants further investigations to unlock its capacity to filter all types of short variations.

We first conducted WTA sequencing using ~5 kb SARS-CoV-2 synthetic controls and R9 flow cells. These standard controls are synthesized according to actual SARS-CoV-2 variants. One limitation is that these controls natively lack true deletion variations in homopolymeric regions, while the false deletion variations are mainly located in homopolymeric regions [23–28]. Trimming bases from both ends of nanopore reads aligned to the reference genome could significantly reduce counts of FP SNVs rather than homo-dels and other-dels, which is consistent with previous studies. The biased distributions of current signals, Q scores, and sequencing speeds between artificial homo-dels and true variations were observed in R9 sequencing data. The high AUC of MRPP A in distinguishing artificial and true variations paved the way for a comprehensive investigation of the characteristics of variations located in homopolymeric regions.

We then synthesized mutant plasmids containing deletion variations in homopolymeric and non-homopolymeric regions relative to wild-type plasmids. We found remarkable differences between reads with and without artificial deletions, with specific preprocessing of raw current signals. As a surrogate of uneven sequencing signals, MRPP A obtained higher AUCs when compared to the Q score and the accumulative sum of normalized signal differences in homopolymeric regions. Notably, the difference is even discernible for the most challenging 1-base homopolymeric deletions, obtaining an AUC >0.8.

Moreover, we investigated the effects of various sequencing depths on distinguishing between FP and TP variations and found that in some cases (strand-specific sequencing depth <400×), the Q score should be applied to filter artificial deletions in R9 sequencing data. When sequencing depth is big enough, the MRPP A and sum of difference values outperformed the Q score in homopolymeric regions (Fig. 5). However, when the sequencing depth decreased, the Q score was more superior. Therefore, it could be indicated that current signal-related indexes were more sensitive to sequencing depth than the Q score.

For R10 sequencing data, the SUP basecalling model generated the least FP deletion variations than the HAC and fast models. Using the Q score alone achieved a better performance than MRPP A, which was used in R9 data. Average Q scores below 22 could separate FP from TP deletions, filtering >90.00% artificial homo-dels and other-dels. The Delter workflow was validated in 2 external datasets composed of paired Illumina and Nanopore R10 se-

quencing runs of the same sample (Table 2). It achieved a 100% accuracy for real deletion variations and filtered 61.43% to 100.00% of FP deletions. Moreover, Delter filters R10 FP deletions using Q-scores, without the need to parse the raw sequencing signals. Thus, Delter needs much less runtime and RAM usage in R10 data than R9 data.

Dorado has now been the default basecaller for ONT data. We re-basecalled the R10 data with the Dorado SUP model (v4.1.0) and analyzed the VCF files output by LoFreq with Delter. It was observed that LoFreq called fewer FP deletion variations in Dorado-basecalled data than in Guppy-basecalled data. Notably, the Delter workflow could filter all the FP deletions in Dorado-basecalled data, which means Dorado can benefit from the filtering procedure employed in Delter (Supplementary Table S10).

Available variant callers like Clair3, Medaka, and NanoCaller, as indicated by Hall et al. [15], were also evaluated using the sequencing data of the synthesized RNA and DNA samples (Supplementary Fig. S15). Clair3 is a state-of-the-art ONT variant caller. However, it calls germline variations, but it is not explicitly designed for intrahost SNV and indel calling. In the context of low-frequency intrahost variation detection (expected MuAF = 0.1, 0.2, and 0.5), LoFreq outperforms the other 3 variant callers. It has the highest recalls and F-scores. Moreover, LoFreq has precision comparable to Clair3. It has been observed that Clair3 calls much fewer true variations than LoFreq. Therefore, LoFreq is more suitable for intrahost variation calling. In the context of high-frequency or consensus-level intrahost variation detection (mutated allele frequency ≥0.8), LoFreq has recall comparable to Clair3 and Medaka but calls more false variations than Clair3 and Medaka. Moreover, Clair3 required less runtime and RAM usage than LoFreq (Supplementary Table S11). In summary, we selected LoFreq to call variations as it balanced recall and precision in the context of low-frequency intrahost variation detection. Notably, Delter could filter FP homo-dels called by Clair3, which indicates Clair3 can benefit from our filtering procedure (Supplementary Table S12).

Until now, few tools could identify artificial indels in nanopore sequencing. One feasible strategy is integrating the datasets from multiple samples collected across different time points or from different patients, as recently reported by Variabel [26]. However, this tool is not suitable for single samples. We believe that our method can break the limit of sample size and facilitate the filtering of false deletion variations in single samples. This study demonstrated that our method can accurately filter low-frequency artificial variations in microbial nanopore sequencing data. It has potential applicability in studies of tumor heterogeneity. One limitation is the lack of ground-truth references for benchmarking such studies. Numerous intrahost variations could always be identified in tumor samples, which need both *in silico* bioinformatic tools and experimental approaches to confirm artificial and true variations.

## Conclusions

By nanopore sequencing of synthetic samples with R9 and R10 flow cells and chemistries, we found that artificial short deletion variations were characterized by differences in current signals and Q scores relative to true variations. The MRPP A or Q score could be employed to filter FP deletions in single samples. The filtering method removed a large proportion of artificial homopolymeric deletions in real samples. We hope the method can facilitate the removal of false variations due to nanopore sequencing errors.

## Availability of Source Code and Requirements

Project name: Delter

Project homepage: <https://github.com/nkuyfq/Delter> [45]

Workflow hub: <https://doi.org/10.48546/workflowhub.workflow.1205.2> [46]

Operating system(s): Linux

Programming language: Python and Perl

Other requirements: Snakemake ( $\geq 7.3$ ) and R ( $\geq 4.2.2$ )

License: MIT license

RRID:SCR\_026376

## Additional Files

**Supplementary Table S1.** The information of SARS-CoV-2 synthetic controls.

**Supplementary Table S2.** The distribution of variations in SARS-CoV-2 synthetic variants against Wuhan-Hu-1 strain.

**Supplementary Table S3.** The information of synthetic DNA samples.

**Supplementary Table S4.** The distribution of deletions in mutant plasmids against wild types.

**Supplementary Table S5.** The distribution of deletions in human adenovirus amplicons and full-length genes against references.

**Supplementary Table S6.** The sequencing summary of synthetic DNA and RNA samples.

**Supplementary Table S7.** The runtime and RAM usage required by LoFreq.

**Supplementary Table S8.** The runtime and RAM usage required by Delter.

**Supplementary Table S9.** The runtime and RAM usage required by basecalling.

**Supplementary Table S10.** The performance of Delter on Dorado-basecalled R10 data.

**Supplementary Table S11.** The runtime and RAM usage required by Clair3.

**Supplementary Table S12.** Validation of the filtering method in deletions called by Clair3.

**Supplementary Fig. S1.** The design of synthetic sequences and mixture samples. (A) The position of deletion variations of the mutated sequences is illustrated as vertical lines. (B) Scheme of mixing the wild types and mutants. The mutant and wild-type plasmids were mixed with 1:9, 1:4, and 1:1 ratios for each mixture.

**Supplementary Fig. S2.** The counts of artificial variations before and after trimming bases in different SARS-CoV-2 variants by 3 variant callers. Only variations with MuAF  $\geq 0.2$  were plotted. Trimnum means the number of trimmed bases.

**Supplementary Fig. S3.** The bar plots of 4 types of artificial variations before (red) and after (blue) trimming bases in R10 direct sequencing samples basecalled with the HAC model (A) and fast model (B). The y-axis was  $\log_{10}$  transformed.

**Supplementary Fig. S4.** The comparisons of Q scores between reads containing deletion variations and reads with no deletions in R10 direct sequencing data basecalled with the HAC model (A) and fast model (B). The dashed lines represent the mean values of Q scores.

**Supplementary Fig. S5.** The comparisons of sequencing speed between reads containing deletion variations and reads with no deletions in R9 WTA sequencing data (A) and R9 direct sequencing data (B) at the scale of the whole read. The dashed lines represented the mean values of speeds. Sequencing speed equals

the division of the number of current measurements by the base number.

**Supplementary Fig. S6.** The features of normalized current signals in R9 sequencing data. (A) Heatmaps of normalized current signals from reads with and without 1-base FP homo-del and 1-base FP other-del variations. The line plots represent each column's average normalized current measurements in the heatmap. The alternate alleles corresponding to deletions are displayed. (B) Heatmaps of normalized current signals from reads with and without 1-base TP homo-del and 1-base TP other-del variations.

**Supplementary Fig. S7.** The accumulative difference of average normalized current measurements from FP and TP deletions stratified by deletion length in R9 WTA sequencing data (A) and R9 direct sequencing data (B). Boxes represent the interquartile range (IQR) between the first and third quartiles (25th and 75th percentiles, respectively). Lines inside denote the median, and whiskers denote the most extreme values within 1.5 times the IQR from the first and third quartiles. Outlier values are represented as points. ns:  $P > 0.05$ , \* $P \leq 0.05$ , \*\* $P \leq 0.01$ , \*\*\*\* $P \leq 0.0001$ . 1b: 1 base; 2b: 2 bases; 3b: 3 bases; 6b: 6 bases; 9b: 9 bases.

**Supplementary Fig. S8.** Performance assessment of different indexes in distinguishing between FP and TP deletions in R9 sequencing data. (A) The ROCs of MRPP A, Q score, and accumulative difference in distinguishing between all FP and TP deletions in R9 WTA sequencing data. (B) The ROCs of MRPP A, Q score, and accumulative difference in distinguishing between all FP and TP deletions in R9 direct sequencing data.

**Supplementary Fig. S9.** The AUCs across different bin numbers of MRPP A, ANOSIM R, and ADONIS2 F in distinguishing between FP and TP deletions in R9 WTA sequencing data (A) and R9 direct sequencing data (B).

**Supplementary Fig. S10.** The ROCs and AUCs of Q score in distinguishing between FP and TP deletions in R10 direct sequencing data basecalled with the fast model.

**Supplementary Fig. S11.** Performance assessment of Q score in distinguishing between FP and TP deletions in R10 direct sequencing samples. (A) The ROC of Q score in distinguishing between FP and TP homo-dels. (B) The ROC of Q score in distinguishing between FP and TP other-dels. The best threshold, specificity, sensitivity, and AUC of the HAC model were plotted.

**Supplementary Fig. S12.** The AUCs distinguishing between TP and FP variations across different sequencing depths. (A) The MRPP A- and Q score-derived AUCs corresponding to all deletions at each sequencing depth in WTA sequencing data. (B, C) The MRPP A- and Q score-derived AUCs corresponding to all deletions (B) and other-dels (C) in R9 direct sequencing data. (D) The Q score-derived AUCs corresponding to all deletions, homo-dels, 1-base homo-dels, and other-dels in R10 direct sequencing data. SumDiff: sum of difference.

**Supplementary Fig. S13.** The runtime and RAM usage required by LoFreq. (A) The runtime as a function of the wall-clock time (seconds) divided by the number of total base pairs (runtime per megabase pairs; y-axis) in each group of samples (x-axis). (B) The runtime as a function of the number of total base pairs in R9 sequencing data. WTA: WTA sequencing of SARS-CoV-2 synthetic RNA controls; Direct: direct sequencing of synthetic DNA plasmids. (C) The runtime as a function of the number of total base pairs in R10 sequencing data of synthetic DNA plasmids that are basecalled with the SUP or HAC model. (D) The maximum memory usage as a function of the maximum memory usage (MB) divided by the number of total base pairs (max memory usage per megabase pairs; y-axis) in each group of samples (x-axis). (E) The



maximum memory usage as a function of the number of total base pairs in R9 sequencing data. WTA: WTA sequencing of SARS-CoV-2 synthetic RNA controls; Direct: direct sequencing of synthetic DNA plasmids. (F) The maximum memory usage as a function of the number of total base pairs in R10 sequencing data of synthetic DNA plasmids that are basecalled with the SUP or HAC model. Boxes represent the interquartile range (IQR) between the first and third quartiles (25th and 75th percentiles, respectively). Lines inside denote the median, and whiskers denote the most extreme values within 1.5 times the IQR from the first and third quartiles. Outlier values are represented as points. \*\*\*\* $P \leq 0.0001$ . Each point represents a single sample. G1: SARS-CoV-2 synthetic RNA controls sequenced with R9 flow cell, WTA sequencing protocol, and basecalled with the SUP model (R9 + WTA sequencing + SUP); G2: synthetic DNA plasmids sequenced with R9 flow cell, direct sequencing protocol, and basecalled with the SUP model (R9 + Direct sequencing + SUP); G3: synthetic DNA plasmids sequenced with R10 flow cell, direct sequencing protocol, and basecalled with the HAC model (R10 + Direct sequencing + HAC); G4: synthetic DNA plasmids sequenced with R10 flow cell, direct sequencing protocol, and basecalled with the SUP model (R10 + Direct sequencing + SUP).

**Supplementary Fig. S14.** The runtime and RAM usage required by Delter. (A) The runtime as a function of the wall-clock time (seconds) divided by the mean number of reads aligned to each deletion variation (runtime per read; y-axis) in each group of samples (x-axis). (B) The runtime as a function of the mean number of reads aligned to each deletion variation in R9 sequencing data. WTA: WTA sequencing of SARS-CoV-2 synthetic RNA controls; Direct: direct sequencing of synthetic DNA plasmids. (C) The runtime as a function of the mean number of reads aligned to each deletion variation in R10 sequencing data of synthetic DNA plasmids that are basecalled with the SUP or HAC model. (D) The maximum memory usage as a function of the maximum memory usage (MB) divided by the mean number of reads aligned to each deletion variation (max memory usage per read; y-axis) in each group of samples (x-axis). (E) The maximum memory usage as a function of the mean number of reads aligned to each deletion variation in R9 sequencing data. WTA: WTA sequencing of SARS-CoV-2 synthetic RNA controls; Direct: direct sequencing of synthetic DNA plasmids. (F) The maximum memory usage as a function of the mean number of reads aligned to each deletion variation in R10 sequencing data of synthetic DNA plasmids that are basecalled with the SUP or HAC model. Boxes represent the interquartile range (IQR) between the first and third quartiles (25th and 75th percentiles, respectively). Lines inside denote the median, and whiskers denote the most extreme values within 1.5 times the IQR from the first and third quartiles. Outlier values are represented as points. \*\*\*\* $P \leq 0.0001$ . Each point represents a single sample. G1: SARS-CoV-2 synthetic RNA controls sequenced with R9 flow cell, WTA sequencing protocol, and basecalled with the SUP model (R9 + WTA sequencing + SUP); G2: synthetic DNA plasmids sequenced with R9 flow cell, direct sequencing protocol, and basecalled with the SUP model (R9 + Direct sequencing + SUP); G3: synthetic DNA plasmids sequenced with R10 flow cell, direct sequencing protocol, and basecalled with the HAC model (R10 + Direct sequencing + HAC); G4: synthetic DNA plasmids sequenced with R10 flow cell, direct sequencing protocol, and basecalled with the SUP model (R10 + Direct sequencing + SUP).

**Supplementary Fig. S15.** Comparison of 4 variant callers in nanopore sequencing data across different mutated allele frequencies. ns:  $P > 0.05$ , \*\* $P \leq 0.01$ , \*\*\* $P \leq 0.001$ , \*\*\*\* $P \leq 0.0001$ .

## Abbreviations

ADONIS2: permutational multivariate analysis of variance; ANOSIM: analysis of similarities; AUC: area under the receiver operating characteristic curve; BAM: Binary Alignment Map; FP: false positive; HAC: high accuracy; HAdV: human adenovirus; Indel: insertion and deletion; MPS: massive parallel sequencing; MRPP: multiresponse permutation procedure; MuAF: mutated allele frequency; Q score: base-quality score; ROC: receiver operating characteristic; SMRT: single molecule real time; SNV: single nucleotide variation; SUP: super accuracy; TP: true positive; VCF: variant call format; WTA: whole transcriptome amplification.

## Author Contributions

M.N. designed the experiments and analysis. J.J.Z., T.T.Y., and Z.H.X. designed synthetic sequences, J.R.Z., Y.F.H., and X.H.Y. conducted the sequencing experiments. F.Q.Y., J.J.Z., and X.M.Z. performed the analysis. F.Q.Y. and Z.L.R. built the workflow. M.N. and F.Q.Y. wrote the draft manuscript and revised the manuscript with contributions of other authors. All authors read and approved the final manuscript.

## Funding

This research was supported by the Incubation Project of Huadong Research Institute for Medicine and Biotechniques (2024YQFH06).

## Data Availability

Nanopore raw data are available from the NCBI BioProjects PRJNA1028169, PRJNA1028529, and PRJNA1140741. The following public sequencing datasets were reused in this study: African swine fever virus (ASFV) dataset: NCBI BioProject PRJNA1096272; *Pseudomonas aeruginosa* PAO1 dataset: EBI Study accession PRJEB51164-ERR8958864 and ERR9285397; *Brucella suis* dataset: EBI Study accession PRJEB59317-ERR10828735 and ERR10820713. Source codes and scripts used to filter artificial deletion variations were integrated into the Snakemake workflow and are available in GitHub [45] and Workflow Hub [46]. Demo data for Delter can be accessed via Figshare [47].

## Competing Interests

The authors declare that they have no competing interests.

## References

1. Li X, Zhang M, Dang C, et al. In situ nanopore sequencing reveals metabolic characteristics of the Qilian glacier meltwater microbiome. *Environ Sci Pollut Res Int*. 2023;30(35):84805–813. <https://doi.org/10.1007/s11356-023-28250-0>.
2. Quick J, Loman NJ, Duraffour S, et al. Real-time, portable genome sequencing for Ebola surveillance. *Nature*. 2016;530(7589):228–32. <https://doi.org/10.1038/nature16996>.
3. Kafetzopoulou LE, Pullan ST, Lemey P, et al. Metagenomic sequencing at the epicenter of the Nigeria 2018 Lassa fever outbreak. *Science*. 2019;363(6422):74–77. <https://doi.org/10.1126/science.aau9343>.
4. Rhie A, Nurk S, Cechova M, et al. The complete sequence of a human Y chromosome. *Nature*. 2023;621(7978):344–54. <https://doi.org/10.1038/s41586-023-06457-y>.

5. Sanderson ND, Kapel N, Rodger G, et al. Comparison of R9.4.1/Kit10 and R10/Kit12 Oxford nanopore flowcells and chemistries in bacterial genome reconstruction. *Microb Genom.* 2023;9(1):mgen000910. <https://doi.org/10.1099/mgen.0.000910>.
6. Zhao W, Zeng W, Pang B, et al. Oxford nanopore long-read sequencing enables the generation of complete bacterial and plasmid genomes without short-read sequencing. *Front Microbiol.* 2023;14:1179966. <https://doi.org/10.3389/fmicb.2023.1179966>.
7. Chen J, Wang Z, Tan K, et al. A complete telomere-to-telomere assembly of the maize genome. *Nat Genet.* 2023;55(7):1221–31. <https://doi.org/10.1038/s41588-023-01419-6>.
8. Sereika M, Kirkegaard RH, Karst SM, et al. Oxford Nanopore R10.4 long-read sequencing enables the generation of near-finished bacterial genomes from pure cultures and metagenomes without short-read or reference polishing. *Nat Methods.* 2022;19(7):823–26. <https://doi.org/10.1038/s41592-022-01539-7>.
9. Aganezov S, Yan SM, Soto DC, et al. A complete reference genome improves analysis of human genetic variation. *Science.* 2022;376(6588):eabl3533. <https://doi.org/10.1126/science.abl3533>.
10. Glinos DA, Garborcauskas G, Hoffman P, et al. Transcriptome variation in human tissues revealed by long-read sequencing. *Nature.* 2022;608(7922):353–59. <https://doi.org/10.1038/s41586-022-05035-y>.
11. Workman RE, Tang AD, Tang PS, et al. Nanopore native RNA sequencing of a human poly(A) transcriptome. *Nat Methods.* 2019;16(12):1297–305. <https://doi.org/10.1038/s41592-019-0617-2>.
12. Shafin K, Pesout T, Chang PC, et al. Haplotype-aware variant calling with PEPPER-Margin-DeepVariant enables high accuracy in nanopore long-reads. *Nat Methods.* 2021;18(11):1322–32. <https://doi.org/10.1038/s41592-021-01299-w>.
13. Lin JH, Chen LC, Yu SC, et al. LongPhase: an ultra-fast chromosome-scale phasing algorithm for small and large variants. *Bioinformatics.* 2022;38(7):1816–22. <https://doi.org/10.1093/bioinformatics/btac058>.
14. van Dijk EL, Naquin D, Gorrichon K, et al. Genomics in the long-read sequencing era. *Trends Genet.* 2023;39(9):649–71. <https://doi.org/10.1016/j.tig.2023.04.006>.
15. Hall MB, Wick RR, Judd LM, et al. Benchmarking reveals superiority of deep learning variant callers on bacterial nanopore sequence data. *eLife.* 2024;13:RP98300. <https://doi.org/10.7554/eLife.98300>.
16. Wang Y, Zhao Y, Bollas A, et al. Nanopore sequencing technology, bioinformatics and applications. *Nat Biotechnol.* 2021;39(11):1348–65. <https://doi.org/10.1038/s41587-021-01108-x>.
17. Chen P, Sun Z, Wang J, et al. Portable nanopore-sequencing technology: trends in development and applications. *Front Microbiol.* 2023;14:1043967. <https://doi.org/10.3389/fmicb.2023.1043967>.
18. Bull RA, Adikari TN, Ferguson JM, et al. Analytical validity of nanopore sequencing for rapid SARS-CoV-2 genome analysis. *Nat Commun.* 2020;11(1):6272. <https://doi.org/10.1038/s41467-020-20075-6>.
19. Liu H, Li J, Lin Y, et al. Assessment of two-pool multiplex long-amplicon nanopore sequencing of SARS-CoV-2. *J Med Virol.* 2022;94(1):327–34. <https://doi.org/10.1002/jmv.27336>.
20. Martignano F, Munagala U, Crucitta S, et al. Nanopore sequencing from liquid biopsy: analysis of copy number variations from cell-free DNA of lung cancer patients. *Mol Cancer.* 2021;20(1):32. <https://doi.org/10.1186/s12943-021-01327-5>.
21. Talsania K, Shen TW, Chen X, et al. Structural variant analysis of a cancer reference cell line sample using multiple sequencing technologies. *Genome Biol.* 2022;23(1):255. <https://doi.org/10.1186/s13059-022-02816-6>.
22. Zheng Z, Su J, Chen L, et al. ClairS: a deep-learning method for long-read somatic small variant calling. *bioRxiv.* 2023. <https://doi.org/10.1101/2023.08.17.553778>.
23. Rang FJ, Kloosterman WP, de Ridder J. From squiggle to basepair: computational approaches for improving nanopore sequencing read accuracy. *Genome Biol.* 2018;19(1):90. <https://doi.org/10.1186/s13059-018-1462-9>.
24. Jain M, Koren S, Miga KH, et al. Nanopore sequencing and assembly of a human genome with ultra-long reads. *Nat Biotechnol.* 2018;36(4):338–45. <https://doi.org/10.1038/nbt.4060>.
25. Cretu Stancu M, van Roosmalen MJ, Renkens I, et al. Mapping and phasing of structural variation in patient genomes using nanopore sequencing. *Nat Commun.* 2017;8(1):1326. <https://doi.org/10.1038/s41467-017-01343-4>.
26. Liu Y, Kearney J, Mahmoud M, et al. Rescuing low frequency variants within intra-host viral populations directly from Oxford Nanopore sequencing data. *Nat Commun.* 2022;13(1):1321. <https://doi.org/10.1038/s41467-022-28852-1>.
27. Delahaye C, Nicolas J. Sequencing DNA with nanopores: troubles and biases. *PLoS One.* 2021;16(10):e0257521. <https://doi.org/10.1371/journal.pone.0257521>.
28. Pages-Gallego M, de Ridder J. Comprehensive benchmark and architectural analysis of deep learning models for nanopore sequencing basecalling. *Genome Biol.* 2023;24(1):71. <https://doi.org/10.1186/s13059-023-02903-2>.
29. Ni M, Chen C, Qian J, et al. Intra-host dynamics of Ebola virus during 2014. *Nat Microbiol.* 2016;1(11):16151. <https://doi.org/10.1038/nmicrobiol.2016.151>.
30. Lythgoe KA, Hall M, Ferretti L, et al. SARS-CoV-2 within-host diversity and transmission. *Science.* 2021;372(6539):eabg0821. <https://doi.org/10.1126/science.abg0821>.
31. Ailloud F, Didelot X, Woltemate S, et al. Within-host evolution of *Helicobacter pylori* shaped by niche-specific adaptation, intragastric migrations and selective sweeps. *Nat Commun.* 2019;10(1):2273. <https://doi.org/10.1038/s41467-019-10050-1>.
32. Vereecke N, Bokma J, Haesebrouck F, et al. High quality genome assemblies of *Mycoplasma bovis* using a taxon-specific Bonito basecaller for MinION and Flongle long-read nanopore sequencing. *BMC Bioinf.* 2020;21(1):517. <https://doi.org/10.1186/s12859-020-03856-0>.
33. De Coster W, D'Hert S, Schultz DT, et al. NanoPack: visualizing and processing long-read sequencing data. *Bioinformatics.* 2018;34(15):2666–69. <https://doi.org/10.1093/bioinformatics/bty149>.
34. Li H. Minimap2: pairwise alignment for nucleotide sequences. *Bioinformatics.* 2018;34(18):3094–100. <https://doi.org/10.1093/bioinformatics/bty191>.
35. Danecek P, Bonfield JK, Liddle J, et al. Twelve years of SAMtools and BCFtools. *Gigascience.* 2021;10(2):giab008. <https://doi.org/10.1093/gigascience/giab008>.
36. Wilm A, Aw PP, Bertrand D, et al. LoFreq: a sequence-quality aware, ultra-sensitive variant caller for uncovering cell-population heterogeneity from high-throughput sequencing datasets. *Nucleic Acids Res.* 2012;40(22):11189–201. <https://doi.org/10.1093/nar/gks918>.
37. Koboldt DC, Zhang Q, Larson DE, et al. VarScan 2: somatic mutation and copy number alteration discovery in cancer by exome sequencing. *Genome Res.* 2012;22(3):568–76. <https://doi.org/10.101/gr.129684.111>.

38. Medaka. Medaka (Version 1.7.3). 2023. <https://github.com/nanoporetech/medaka/releases/download/v1.7.3/medaka-1.7.3.tar.gz>. Accessed 7 Dec 2024.
39. Zheng Z, Li S, Su J, et al. Symphonizing pileup and full-alignment for deep learning-based long-read variant calling. *Nat Comput Sci*. 2022;2(12):797–803. <https://doi.org/10.1038/s43588-022-00387-x>.
40. Ahsan MU, Liu Q, Fang L, et al. NanoCaller for accurate detection of SNPs and indels in difficult-to-map regions from long-read sequencing by haplotype-aware deep neural networks. *Genome Biol*. 2021;22(1):261. <https://doi.org/10.1186/s13059-021-02472-2>.
41. ont\_fast5\_api. [https://github.com/nanoporetech/ont\\_fast5\\_api](https://github.com/nanoporetech/ont_fast5_api). Accessed 20 Dec 2024.
42. R. R (Version 4.2.2). 2022. <https://cloud.r-project.org/bin/windows/base/old/4.2.2/R-4.2.2-win.exe>. Accessed 20 Dec 2024.
43. ggsci. ggsci (Version 2.9). 2018. <https://github.com/nanxstats/ggsci/archive/refs/tags/v2.9.tar.gz>. Accessed 20 Dec 2024.
44. Lin HN, Hsu WL. GSAAlign: an efficient sequence alignment tool for intra-species genomes. *BMC Genomics*. 2020;21(1):182. <https://doi.org/10.1186/s12864-020-6569-1>.
45. Ye F, Zhu J, Zhang X, et al. ONT Artificial Deletion Filter-Delter (Version 1). [Computer software]. Software Heritage. 2025 <https://archive.softwareheritage.org/swh:1:snp:79430faf1a78289783766d1714a5de0141647ed5;origin=https://github.com/nkuyfq/Delter>. Accessed 8 Feb 2025.
46. Ye Q. ONT Artificial Deletion Filter-Delter. WorkflowHub. 2024. <https://doi.org/10.48546/WORKFLOWHUB.WORKFLOW.1205.2>. Accessed 20 Dec 2024.
47. Ye Q. Example dataset containing Fast5 and BAM files. figshare. Dataset. 2024. <https://doi.org/10.6084/m9.figshare.26093869.v5>. Accessed 20 Dec 2024.